Self-Consistent Calculation of Electron Transport in a Cylindrical Hall Thruster

Lubos Brieda*, Michael Keidar†
The George Washington University, Washington, D.C. 20052
Yevgeny Raitses and Nathaniel J. Fisch
Princeton University Plasma Physics Laboratory, Princeton, NJ 08543

In this paper, we investigate electron transport in the Princeton Cylindrical Hall thruster using a one-dimensional electron kinetic code. The code self-consistently computes plasma properties along a magnetic field line. Ion and neutral densities, as well as the normal component of the electric field are obtained from hybrid code HPHall. In our analysis, we investigated the effect of near-wall conductivity on transport. We computed the radial variation in transport for two magnetic field lines, and found a significant contribution from NWC along one of the field lines.

I. Introduction

The classical model of a Hall thruster is based on electron conduction across magnetic field lines being driven by electron collisions with heavy particles (ions and neutrals). However, this model does not explain the high anode currents observed experimentally. Understanding this "anomalous" diffusion is important from several standpoints. First, anode current is directly related to the overall thruster efficiency. Electrons that escape the confinement do not contribute towards ionizing the working gas, and thus the energy used to create them is wasted. Secondly, distribution of electrons influences the structure of plasma potential inside the device. It is this potential which acts, through the electric field, to accelerate the ions and thus produce thrust. Detailed understanding of electron transport is thus necessary in order to improve the performance of these devices. Current Hall thruster simulation codes resort to incorporating various mobility correction factors to account for this anomalous diffusion. These factors vary greatly between thrusters and operating conditions, and thus the existing numerical tools are of limited use for predictive modeling of these devices.

The classical diffusion model states that cross-field transport is due to electron collisions with ions and neutrals. However, the close proximity of walls inside the Hall thruster leads to an additional transfer mechanism due to scattering wall interactions. Electron with sufficient energy to penetrate the sheath and impact the dielectric wall can either reflect back, or kick off another electron from the surface. Of interest here are the diffuse wall collisions, and the secondary electron emissions (SEE). The difference between these two processes is that SEE acts to cool the electron population,[1] since their initial temperature corresponds to that of the wall. However, of importance in this paper is their identical role on transport, as they both diffuse the electron onto a new magnetic field line. Collectively, these two effects are known as *near-wall conductivity*.

In order to investigate electron transport, we have constructed a simulation code which directly resolves the orbital motion of electrons along a magnetic field line. The simulation domain consisted of a single magnetic field line bounded by two dielectric walls. Only electrons were simulated. Sheath drop was computed self-consistently from the Poisson equation. This approach is similar to the previous work of Sydorenko[1] with the notable exception that we have taken into account the spatial variation of magnetic

*PhD Candidate, Department of Mechanical and Aerospace Engineering, lbrieda@gwu.edu
†Assistant Professor, Department of Mechanical and Aerospace Engineering, keidar@gwu.edu

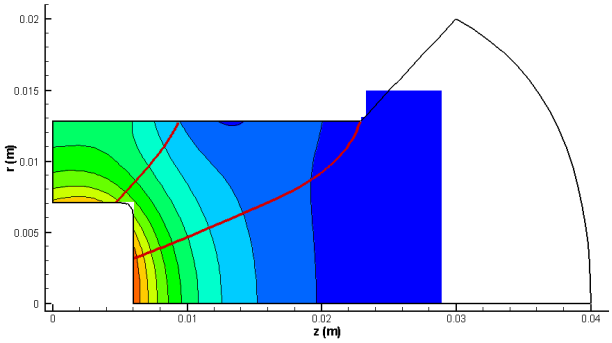

Figure 1. Plot of the computational domain. Two representative field lines are shown by thick black line. We considered the right-most line in the kinetic simulation. The black boundary corresponds to the domain used by HPHall. Contours show the magnitude of the magnetic field.

field. In addition, we have implemented method based on guiding center shifts to characterize the radial variation in transport in order to study the effect of NWC.

We applied the code to the 2.6 cm Princeton cylindrical Hall thruster (CHT). This device, which is characterized in detail in Ref. 2, consists of a short annular anode region and a longer cylindrical acceleration zone. The channel walls are made of Boron Nitride and Xenon is used as the working gas. The measured discharge current for the configuration studied in this paper was approximately 0.3 A. The device geometry leads to an interesting field configuration not seen in the traditional annular Hall thrusters. The convergence of field lines near the upstream end of the cylindrical region results in a magnetic field gradient. The mirroring effect is expected to reduce the flux of electrons to this wall. The strength of the magnetic field is shown in Figure 1. This figure also illustrates the two field lines analyzed in our work.

Since our code tracked only electrons, we needed a radial distribution of ions and atoms in order to compute the plasma potential and to model collisions. Experimental measurements were not available at the required resolution. Hence, we utilized HPHall, a 2D axi-symmetric code for Hall thruster discharges, to model the plasma properties inside the thruster. The simulation results were used as inputs to the kinetic code. HPHall is described in more detail in the next section. The following sections then describe the kinetic code, and give simulation results.

II. Hall Thruster Simulation

HPHall is an axi-symmetric hybrid code developed by Fife[3] to investigate plasma properties of the SPT-70 thruster. Since then, the code has been applied to various thruster designs.[4–6] HPHall uses the particle-in-cell method for the heavy particles. Plasma is assumed to be quasi-neutral. Electrons are modeled as 1D fluid. The axial variation in potential is computed by solving conservation equations along the thruster centerline. Electron temperature is assumed to remain constant along each magnetic field line. Under this assumption, the radial variation in potential is given by the thermalized model, $\phi^* = \phi - \frac{kT_e}{e}\ln(n_e)$.

HPHall solves the fluid equations only between the anode and the cathode. The position of the cathode boundary is one of the parameters affecting the potential distribution inside the device.[6] It should be noted that this "cathode position" generally does not correspond the location of the physical cathode. In our work, we tested three cathode boundary conditions. The cathode positions were z=6.7, 7.6 and 8.7 cm, with the anode located at 4.9cm. The values of potential and electron temperature were obtained from measurements in Refs. 7 and 8. The sampled values were 6eV and 210V, 21.6eV and 128V, and 12eV and 60V, respectively. Electron density at the cathode was set to 10^{18} m^{-3}. The coefficient for the anomalous Bohm diffusion was varied from 0.5 to 1.2. This range was similar to the previous work of Garrigues,[9] in which the value of 0.8 was used. Thruster operating condition was 250V of discharge voltage and propellant flow rate of 0.4mg/s. Chamber back pressure was 9mPa (6.7×10^{-5} Torr).

Axial variation of plasma potential and plasma density is shown in Figure 2. The two vertical lines indicate the extent of the cylindrical region. The code obtained an excellent agreement with potential and temperature measurements inside the thruster. However, the agreement with plasma density is not good, and the code underpredicts electron density by several orders of magnitude. This discrepancy can be attributed to

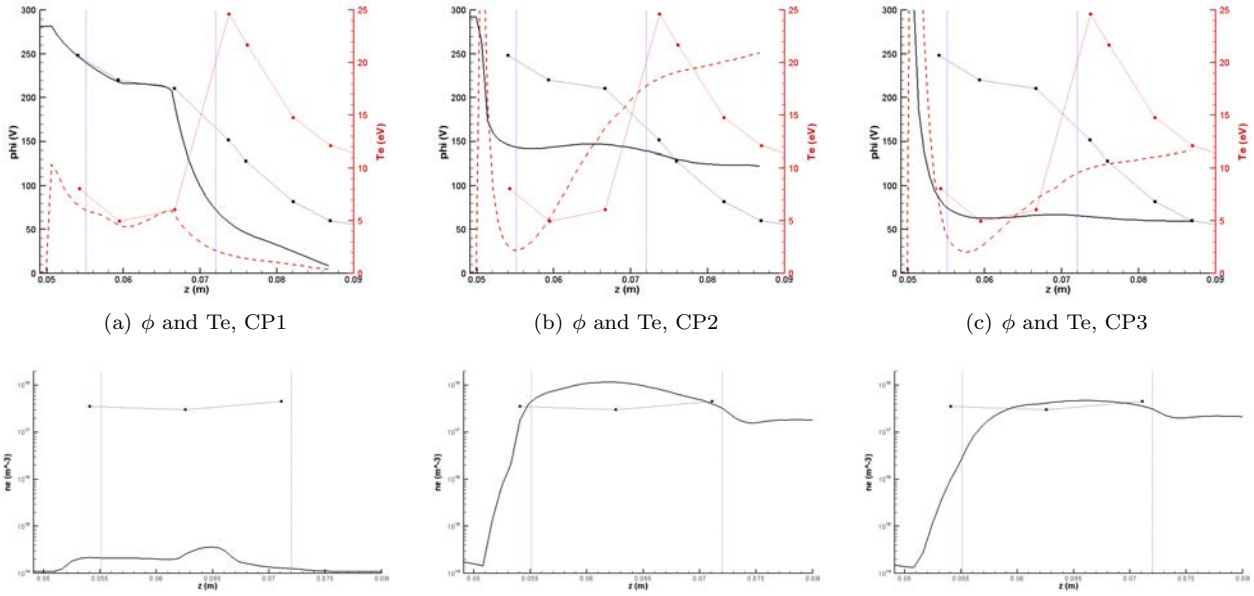

(a) ϕ and Te, CP1 (b) ϕ and Te, CP2 (c) ϕ and Te, CP3

(d) Plasma Density, CP1 (e) Plasma Density, CP2 (f) Plasma Density, CP3

Figure 2. Axial variation in plasma properties for the three considered cathode positions. The cathode position is a simulation boundary condition and does not correspond to the location of the physical cathode. The dashed lines correspond to experimental measurements from Refs. 7 and 8.

low ionization rate due to the low prescribed electron temperature. Hence, we performed another simulation with the boundary values identical to the CP1 case. However, electron temperature was artificially increased to 21.6eV, corresponding the temperature measured at the CP2 location.

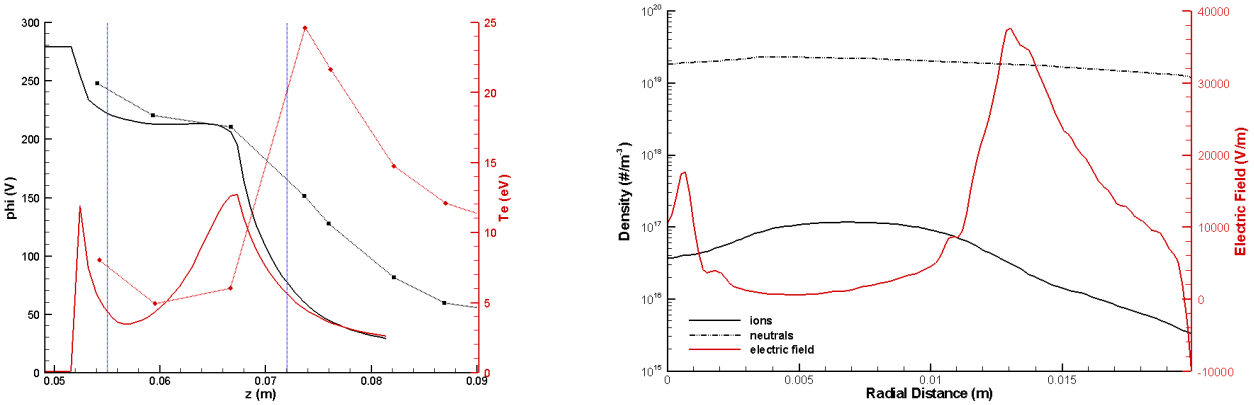

(a) Potential and Temperature (b) Cathode Line Properties

Figure 3. HPHall results obtained with adjusted cathode temperature. Figure (b) shows the variation along the field line in parameters used as inputs to the kinetic code

Figure 3(a) shows the resulting potential and temperature. Electron density increased to 10^{17} m^{-3}. The variation of properties of interest along the $\Lambda 2$ field line is shown in Figure 3(b). along the magnetic field line. Neutral density ranges from 1.2×10^{19} to 2.3×10^{19} m^{-3}. Ion density range is 3.3×10^{15} to 1.2×10^{17} m^{-3}. The normal component of electric field reached 33 kV/m. The magnitude of the field along the outer dielectric wall was approximately -10 kV/m. The anode current predicted by HPHall for this configuration was 0.008A, under-predicting the experimentally measured current by a factor of 37.

III. 1D Kinetic Code

A. Overview

The kinetic code was based on the particle-in-cell (PIC) method. Electrons were simulated as computational macro-particles. All three components of velocity and position were retained, however, plasma parameters varied only in one-dimension along the field line. Acceleration, given by the Lorentz force, $F = q\left(\vec{E} + \vec{u} \times \vec{B}\right)$, was integrated using the 4-step Boris method. Particle position was computed using the Leapfrog method. This method was chosen over Runge-Kutta, as it provided comparable accuracy at a fraction of the computational overhead. The initial distribution of electrons was obtained from the ion density, which was converted to particle count by multiplying by the cell volume and scaling by the macroparticle weight. However, in the sheath region, electron and ion densities deviate from quasi-neutrality. As such, the total ion charge in the slab contained between the two walls exceeds the total electron charge, $q_e = \kappa q_i$, where $\kappa < 1$. The ratio κ can be estimated numerically. Ion density in the sheath is given by $n_i = n_s\left(1 - 2e\phi/Mu_b^2\right)^2$, where u_b is the Bohm velocity. Electron density decays according to the Boltzmann relation, $n_e = n_s \exp\left(\phi/kTe\right)$. Potential variation is obtained by integrating the 1D Poisson equation, $\epsilon_0 \mathrm{d}^2\phi/\mathrm{d}x = q(n_e - n_i)$. The domain length corresponded to half the length of the magnetic field line, with $\phi(0) = \phi_w$ and $\phi(L/2) = 0$. The sheath potential drop is given by[10] $\phi_w = \ln(2\pi m_e/M)^{1/2}T_e$, or $\phi_w = -5.27T_e$. We obtained $\kappa = 0.9762$ for the first magnetic field line and 0.9858 for the second line.

Electrons were loaded with random tangential and normal velocity components. The velocities came from sampling the Maxwellian distribution at 3.6eV for $\Lambda 1$ and 10eV for $\Lambda 3$. These temperatures corresponded to the averaged value obtained from HPHall. At each time step, plasma potential was computed along the field line by a direct Poisson solver. Both ends of the computational domain were fixed at $\phi = 0$V. Electric field was obtained from $E_{\|} = -\partial\phi/\partial r$. Plot of a characteristic potential profile is shown in Figure 4. This figure also shows a typical velocity distribution profile at the end of the simulation. It should be noted that the potential solution develops initial oscillations, which are due to the finite particle loading. This effect is also demonstrated by the noise in the density data. We attempted to reduce these oscillations by increasing the number of computational particles and reducing the simulation time step.

Since we were interested in resolving the non-neutral sheath, we set the cell size as $\Delta r = 0.5\lambda_D$. Number of simulation cells was 1120. Time step was set by considering orbital and translational motion of electrons. The time step used in the simulation was 7.3×10^{-13}s. At this temporal resolution, an electron completed a cyclotron orbit every 360 steps. Electron oscillations were resolved, and electrons took about 28 time steps to traverse through a cell. Simulation consisted of 300,000 particles (approximatelly 270 particles per cell). Total of one million time steps were simulated. The simulation was performed serially using the 1048-node Sun X2200 M2 Pyramid cluster at The George Washington University.[11] Each case took approximately 6 hours to complete.

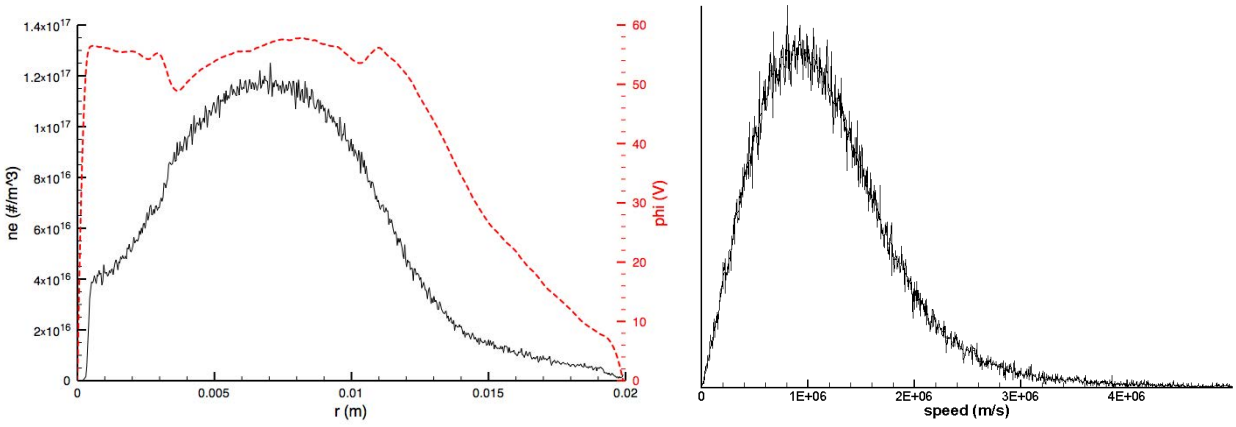

(a) Potential and Electron Density

(b) Distribution Function

Figure 4. Plot of typical instantaneous simulation results, showing the variation in plasma potential, electron density, and the speed distribution function.

B. Collisions

Electron collisions were modeled using the Monte Carlo method. In this method, source particles are collided with a stationary target cloud. The collision probability is determined from background density, n_0 and collision frequency is $P = 1 - \exp(-n_0 \sigma_0 g \Delta t)$. Here σ_0 is the total collision cross-section due to all processes. For particles undergoing collision, the collision process was picked randomly according to the ratio of σ_i/σ_0. Post-collision velocity was computed by first sampling a random target velocity and a random impact angle. We then calculated the post-collision velocity from conservation of energy.

Collision frequency is several orders of magnitude lower than the cyclotron frequency. In order to reduce numerical errors, collisions were performed only once per orbit. Four types of collisions were considered: momentum-transfer (electron-atom), Coulomb (electron-electron and electron-ion), ionization (electron-atom) and excitation (electron-atom). At low electron temperatures, polarization collisions dominate the momentum-transfer interaction between electrons and atoms.[10] Cross-section for this process was obtained from the analytical model[10]

$$\sigma_{Xe} = \left(\frac{\phi \alpha_p q^2}{\epsilon_0 m} \right)^{1/2} \frac{1}{v} \tag{1}$$

where α_r is the polarizability of the atom. It is given by $\alpha_r = 27.66 a_0^3$, where a_0 is the Bohr radius.[12] Cross-section for electron-ion collisions was given by

$$\sigma_{Xe^+} = \frac{8}{\pi} b_0^2 \ln \Lambda \tag{2}$$

where $b_0 = q_1 q_2/(2\pi\epsilon_0 m v^2)$ is the distance of closest approach. The inelastic process, ionization and excitation, cross-sections were computed using the polynomial fit of Szabo.[13] The direction of impacting electrons was replaced by a randomly sampled vector. Energy of the particle was reduced by either the ionization energy, or by a random value with the upper bound at the ionization energy for the excitation collision.

C. Wall Effects

Electrons impacting the dielectric walls were reflected back into the simulation domain. No thermal accommodation was performed. However, in order to analyze the effect of surface roughness on transport, we implemented a roughness parameter k_s, which specified the probability a particle will be scattered by the wall. We considered two values, 0 (perfectly smooth surface) and 0.5 (half of impacting particles diffuse). Scattered particles were reflected into the simulation domain by sampling a random velocity vector.

Electron impact also contributes to emission of secondary electrons (SEE) from the wall. The yield scales with the energy of the impacting particles, E_p. We used the linear fit of experimental measurements given by Dunaevsky[14] as,

$$\gamma = \left(\frac{E_p}{35\text{eV}} \right)^{0.5} \tag{3}$$

The SEE yield is non-negligible for $kTe = 10$eV. The SEE electrons were assumed to come off the surface unmagnetized, and were generated at the wall with initial direction given by a random velocity vector. Impacting electron knocking off a secondary electron was assumed to be absorbed by the wall to retain charge neutrality, and was removed from the simulation.

D. Drifts

The crossed E and B configuration yields to drift of electrons in the direction perpendicular to both fields. In a Hall thruster, this $E \times B$ drift is oriented in the azimuthal direction, and hence does not contribute to anode current. Similar azimuthal drifts arise from curvature and gradient of the magnetic fields. However, due to the geometry of the cylindrical Hall thruster, the magnetic field develops a strong gradient in the tangential direction. This effect can be seen from the plot magnetic field magnitude, with the maximum effect observed near the upstream end of the cylindrical region. Conservation of magnetic moment dictates that perpendicular velocity of electrons must increase as the particles move to the region of stronger magnetic field. This in turn has the effect of reducing the tangential velocity in order to conserve particle's energy. The field line considered in this work intersects this region. As such, we expect reduced wall interaction near

the center-pole due to the magnetic mirror effect. The tangential force acting on a particle as it travels into a region of increasing magnetic strength was given by

$$F_z = \frac{mv_\perp^2}{2B_z}\frac{\partial B_z}{\partial z} \tag{4}$$

E. Transport Calculation

We utilized two methods to characterize electron transport. First, we computed overall mobility from $\mu = v_d/\bar{E}_\perp$. Here $\bar{E}_\perp$ is the average perpendicular component of the electric field. The average drift velocity was computed by collecting the x-component of velocity of particles at each time step. This method was not used to characterize the radial variation in transport, due to presence of statistical errors associated with the tangential drift of electrons and presence of regions with small magnitude of $\bar{E}_\perp$.

We computed the spatial variation in current from shifts of particle guiding centers. Viewed in the direction tangent to the field line, the particle trajectories form circles drifting in the $+y$ direction (due the $\vec{E} \times \vec{B}$ drift). Disregarding this azimuthal drift, we can compute the x component of the guiding center from $x_g = 0.5(x^+ + x^-)$. Particle has left the field line if x_g has drifted by a distance greater than some fraction of the Larmor radius, $|x_g - x_0| > gr_L$. In our work, we used $g = 1$, but we also investigate the effect of this parameter on results. Larmor radius was computed directly from the tangential velocity. Only particles traveling towards the anode ($x_g < 0$) were considered. The diffused particles were removed from the simulation, and new particles were sampled at random position along the field line. Total current was calculated by integrating the linear current density over the annular area swept by the field line.

F. Code Validation

The code was validated through a set of unit-tests. Particle integrator was tested by verifying energy conservation by integrating velocity of a particle for one million time steps. Potential solver was tested by using charge density variation with a known analytical solution. Collision frequency was compared with theory based on mean particle velocity and mean gas densities. Collisions were also used to characterize the transport algorithm. In this test, we loaded uniform ion density, $n_i = 10^{18}$ m^{-3}. Neutral density was zero. Collisions were represented by the hard-sphere model, $\sigma = 10^{-18}$ m^2. Electrons were loaded with $v_\perp = 10^6$m/s. Constant $E_\perp = 10,000$ V/m and $B_\parallel = 0.01$ T were also applied. Potential solver, SEE, and surface scatter were disabled. Collision frequency is $\nu = \tau^{-1} = n_i\sigma\bar{v} = 10^6$ Hz. Cyclotron frequency is $\omega_c = |q|B/m = 1.8 \times 10^9$ Hz. Mobility in the absence of magnetic confinement is defined as $\mu = |q|/m_e\nu = 1.8 \times 10^5$ T^{-1}. The cross-field mobility is then given as

$$\mu_\perp = \frac{\mu}{1 + \omega_c^2\tau^2} \tag{5}$$

or $\mu_\perp = 0.057$ T^{-1}. Next, the drift velocity was computed, $v_d = \mu_\perp E_\perp = 568$m/s. Current is then given by $I = n_i q v_d A$, where A is the area swept by the field line. The theoretical value for the given inputs is $I = 0.15A$. The kinetic code predicted $I = 0.361A$. The two values agree within an order of magnitude. Drift velocity was calculated as $v_d = 69$m/s, under-predicting theory by an order of magnitude. Source of this discrepancy remains to be investigated.

IV. Results

Figure 5(a) shows the calculated tangential variation in transport for the first magnetic field line. The y axis in this plot corresponds to the total charge of particles moving towards the anode at the sampling location, divided by the total sampling time. The x axis is the distance along the field line. The red line shows the result obtained after all factors contributing to near-wall conductivity (surface roughness and SEE) were switched off. As such, the difference between the two results corresponds to the contribution from NWC. Transport is concentrated in three distinct regions: zone near the inner wall, channel-zone dominated by collisions, and a narrow band due to SEE near the outer wall. The shift of the near-wall transport away from the walls is due to the sampling process. Transport was computed only every 5 orbits. During which time the electron moved along the field line. The width of these two peaks thus corresponds to the variation in tangential velocities of the NWC electrons.

As expected, NWC played a significant role on transport in the first field line. However, along the second field line, the effect of NWC was negligible. The radial transport for this case is shown by Figure 5(b). Here the transport is concentrated in the channel centerline, approximately in the region of maximum perpendicular electric field. The transport is expected to be collision-driven, but the exact mechanism remains to be investigated. Total current was calculated numerically by integrating this linear current over the area swept by the field line. The integrated current is summarized in Table 1.

Case	Current (A)
L1, NWC	9.8×10^{-4}
L1, no NWC	9.1×10^{-4}
L2, NWC	0.436
L2, no NWC	0.436

Table 1. Integrated current for the four studied cases.

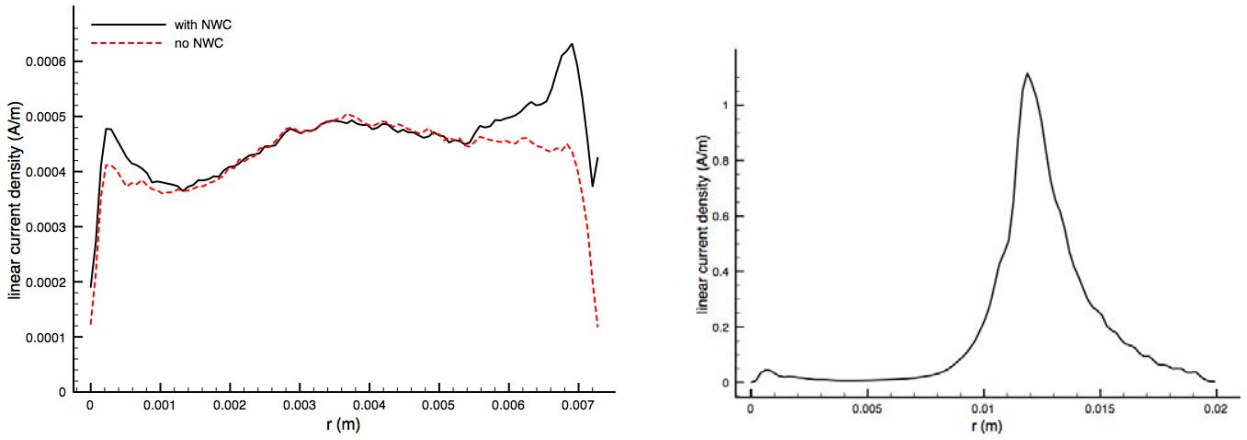

(a) Transport (b) Integrated Current

Figure 5. Simulation results, showing the spatial variation in transport for the two magnetic field lines. Clear influence of NWC is seen for line 1. However, NWC seemed to play negligible role at the second field line.

We further investigated the influence of the sampling radius on transport. This analysis was performed only for the second field line, and the results are summarized in Figure IV. As expected, increasing the threshold radius decreases the collected current. However, of importance is that this variation has only negligible effect on the quantitative description of mobility. The slight shift in the tangential position of peak current is only observed for $\kappa < 1$ and may correspond to numerical noise.

The drift velocity obtained from the code was 73 m/s for the first field line. This low speed is analogous to the low collected anode current. At the second field line, the drift velocity increased to 200,000 m/s. The corresponding mobility, $\mu = \bar{E}_\perp m/v_d$, is approximately 20. Although our code predicted current in line with experimental measurements at the second field line, the current was underestimated at the first cathode position by 2 orders of magnitude. Additional work, taking into accounts other effects such as field oscillations, is clearly needed in order to improve the agreement. We estimated the magnitude of the anomalous coefficient using the definition of Bohm mobility used in HPHall. Cross-field mobility in HPHall is defined as

$$\mu_\perp = \frac{q}{m}\frac{\nu_m}{\omega_c^2} + K_B\frac{1}{16B} \tag{6}$$

where the first term on the RHS corresponds to the classical diffusion. K_B is the anomalous Bohm diffusion coefficient. Using the average values of B, $E_\perp$ and n_e of 0.06T, 1980 V/m and 5.6×10^{16} m^{-3}, respectively, we obtain $\mu_{\perp,c} = 3.2$ T^{-1}. Here we added the subscript $_c$ to indicate the classical diffusion. However, from $I_a = Aqnev_d$, we can estimate the drift velocity corresponding to the experimentally measured current to be $v_d = 23,900$ m/s. Mobility, computed using the average value of $E_\perp$ is then $\mu_x = 12.06$ T^{-1}. The

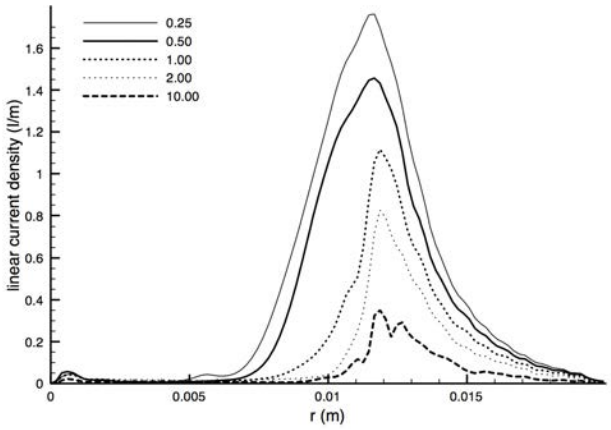

Figure 6. Figure showing the effect of Larmor radius scaling factor, κ, on computed transport.

discrepancy between these two results correspond the "anomalous" Bohm term, $K_B/16B$. Using these values in Eq. 6, we obtain $K_b = 8.5$.

V. Conclusion

In this paper we used a kinetic code to investigate transport in the Princeton cylindrical Hall thruster. Our code predicted anode current in a reasonable agreement with the experimental measurements. Results indicate that near wall conductivity plays an important role in electron transport. Transport due to secondary electron emission was concentrated on the outer wall due to the strong magnetic mirroring effect near the upstream end of the cylindrical zone. We used the calculated mobility to estimate the anamalous diffusion coefficient. Source of this anomaly remains to be investigated. Future work will include detailed optimization of HPHall input parameters and coupling of calculated Bohm mobility with HPHall.

VI. Acknowledgments

The authors would like to thank Dr. Justin Koo at the Air Force Research Laboratory for valuable discussion and assistance in constructing the HPHall mesh.

References

[1]Sydorenko, D., Smolyakov, A., Kaganovich, I., and Raitses, Y., "Modification of Electron Velocity Distribution in Bounded Plasmas by Secondary Electron Emission," *IEEE Transactions on Plasma Science*, Vol. 34, No. 3, 2006, pp. 815–824.

[2]Smirnov, A., Raitses, Y., and Fisch, N., "Parametric investigation of miniaturized cylindrical and annular Hall thrusters," *Journal of Applied Physics*, Vol. 92, 2002, pp. 5673.

[3]Fife, J. M., *Hybrid-PIC Modeling and Electrostatic Probe Survey of Hall Thrusters*, Ph.D. thesis, Massachusetts Institute of Technology, Cambridge, MA, 1998.

[4]Hofer, R., Mikellides, I., Katz, I., and Goebel, D., "BPT-4000 Hall Thruster Discharge Chamber Erosion Model Comparison with Qualification Life Test Data," *30th International Electric Propulsion Conference*, 2007, pp. 2007–267.

[5]Ahedo, E., Maqueda, I., Antón, A., Raitses, Y., and Fisch, N., "Numerical simulations of a 2kW Hall thruster," *42th Joint Propulsion Conference, Sacramento, CA*, 2006, pp. 2006–4655.

[6]Nakles, M., Hargus, W., and VanGilder, D., "Comparison of Numerical and Experimental Near-Field Ion Velocity Distributions of the BHT-200-X3 Hall Thruster," *42nd Joint Propulsion Conference, Sacramento, CA*, 2006, AIAA-2006-4479.

[7]Raitses, Y., Smirnov, A., and Fisch, N., "Effects of enhanced cathode electron emission on Hall thruster operation," *Physics of Plasmas*, Vol. 16, 2009, pp. 057106.

[8]Smirnov, A., Raitses, Y., and Fisch, N. J., "Plasma measurements in a 100W cylindrical Hall thruster," *Journal of Applied Physics*, Vol. 95, No. 5, 2004, pp. 2283–2291.

[9]Garrigues, L., Hagelaar, G. J. M., Boeuf, J. P., Raitses, Y., Smirnov, A., and Fisch, N. J., "Two Dimensional Hybrid Model of a Miniaturized Cylindrical Hall Thruster," *30^{th} International Electric Propulsion Conference*, Florence, Italy, 2007, IEPC-2007-157.

[10]Lieberman, M. and Lichtenberg, A., *Principles of plasma discharges and materials processing*, Wiley-interscience, 2005.

[11] "Institute for Massively Parallel Applications and Computing Technologies," http://hpcl.seas.gwu.edu/impact/.

[12] Nicklass, A., Dolg, M., Stoll, H., and Preuss, H., "Ab initio energy-adjusted pseudopotentials for the noble gases Ne through Xe: Calculation of atomic dipole and quadrupole polarizabilities," *Journal of Chemical Physics*, 1995.

[13] Szabo Jr, J., *Fully kinetic numerical modeling of a plasma thruster*, Ph.D. thesis, Massachusetts Institute of Technology, 2001.

[14] Dunaevsky, A., Raitses, Y., and Fisch, N., "Secondary electron emission from dielectric materials of a Hall thruster with segmented electrodes," *Physics of Plasmas*, Vol. 10, 2003, pp. 2574.